Advances in Artificial Intelligence and Machine Learning; Research 6 (4) 6086-6107 Received 20-05-2026; Accepted 19-08-2026; Published online 26-08-2026

Effect of Degradations Introduced by Imaging Systems in Patch-Based Machine Learning for Mammogram Cancer Detection

Santoresh Kumari Dhimann santoreshlehana@gmail.com
Department of Computer Science & Engineering
Maharishi University of Information Technology
Lucknow, India

Rakesh Kumar Yadav rkymuit@gmail.com
Department of Computer Science & Engineering
Maharishi University of Information Technology
Lucknow, India

Corresponding Author: Santoresh Kumari Dhimann

Abstract

Machine learning-based breast cancer detection from mammograms is inherently affected by image degradation induced by imaging systems. Conventional algorithms mainly target enhancement of classification performance in an ideal imaging scenario; little consideration is generally given to the impact of imaging degradations on robustness and interpretability of the model. In this paper, a robust approach for systematically investigating the effect of essential imaging system features, such as spatial resolution, image blur, and additive Gaussian noise concerning patch-based mammogram cancer detection has been introduced. A convolutional neural network combined with a circular attention mechanism is used to extract discriminative features from fixed-size mammogram patches and provide an interpretable visualization. The model is trained on high-quality, non-degraded patches and is evaluated on degraded patches to investigate the effect of different imaging factors. The proposed system incorporates patch-based learning, degradation modeling, quantitative performance evaluation, lesion localization analysis, and attention-based interpretability within the developed framework to formulate an integrated evaluation of the model functionality under realistic acquisition environment. Experimental results indicated that spatial resolution was the most crucial factor for detection performance, and even modest resolution degradation brought a major drop in cancer sensitivity, lesion localization performance, and attention-map quality. The investigations also showed that the model is relatively robust for mild Gaussian blur and moderate Gaussian noise. It was noted that blur primarily affects edges and texture of the processed mammograms whereas noise mostly diminishes classification specificity by inducing false positive outputs and preserving lesion detectability. Attention visualizations showed that imaging degradations decrease feature localization and diminish the ability of the network to focus on areas important for diagnosis. The research emphasizes the importance of image quality for reliable mammogram analysis using machine learning. Further, it shows that the traditional accuracy metrics results in lower diagnostic integrity. Thus, the proposed

Citation: Santoresh Kumari Dhimann and Rakesh Kumar Yadav. Effect of Degradations Introduced by Imaging Systems in Patch-Based Machine Learning for Mammogram Cancer Detection. **Advances in Artificial Intelligence and Machine Learning**. 2026;6(4):337. https://dx.doi.org/10.54364/AAIML.2026.64337

framework results in the development of robust, interpretable, and clinically implementable computer-aided diagnosis systems for breast cancer detection particularly for rural clinics where access to high-end imaging systems is generally limited.

Keywords: Breast cancer detection, Mammography, Deep learning, Convolutional neural network, Circular attention, Image quality assessment, Image degradations, Spatial resolution, Gaussian blur, Gaussian noise.

1. INTRODUCTION

Breast cancer is one of the most common fatal diseases for women worldwide, accounting for a substantial percentage of cancer-related morbidity and mortality. Early screening, particularly mammography, is a well-established technique to reduce breast cancer mortality. Mammographic imaging, including conventional two-dimensional (2D) digital mammography and three-dimensional (3D) digital breast tomosynthesis (DBT), delivers detailed images of breast tissue structures where abnormalities such as masses, calcifications, and structural distortions are required to be precisely analysed by radiologists at the early stages for proper treatment. As illustrated in FIGURE 1, mammogram acquisition is the initial stage of the breast cancer screening where several factors associated with the acquisition and imaging technology affects the mammogram quality. High quality mammograms are important for reliable diagnosis and visualization of lesions adequately. However, interpretation of the mammograms still can be laborious, time-consuming, and prone to inter-observer variability. This may lead to diagnostic errors, especially in dense breasts where fine changes may be difficult to detect. Computer-aided diagnosis (CAD) systems are assumed to overcome such challenges. They are expected to enhance the diagnostic accuracy, consistency, and efficiency. The performance of the CAD systems can further be enhanced using machine learning for mammogram interpretation and diagnosis. Machine learning has been improving rapidly for the last several years, which led to an extremely significant transformation of medical image analysis, allowing for the development of accurate and automated breast cancer detection systems.

Figure 1: Proposed Robustness-Aware Patch-Based Deep Learning Framework for Investigating the Impact of Imaging System Degradations on Mammogram Cancer Detection

Convolutional neural networks (CNNs) have shown encouraging results in classification and detection of features having excellent discriminative abilities [1]. Yann Le Cun has developed a gradient based CNN architecture, later improved by Kaiming He through deep residual learning using skip connections to tackle the vanishing gradient problem in deep learning systems, for finding complex visual patterns [2–4]. Huang et al. (2017) [5], modified conventional CNN by connecting each layer to every other layer in a feed-forward manner to strengthen feature propagation and reduce the number of parameters, to enhance feature reuse and gradient flow in deep CNNs. The advancements have been successfully applied to medical imaging, achieving performance comparable to expert radiologists in breast cancer detection [6, 7] and extended to histopathology analysis for cancer diagnosis [8, 9]. Recently, patch-based approaches have gained considerable attention for mammogram analysis and cancer detection. Instead of processing entire high-resolution images, these methods divide mammograms into smaller regions, allowing models to focus on localized features that are critical for detecting abnormalities such as microcalcifications and other type of masses in the mammograms. Dieter Ribli has reported the effectiveness of CNNs in detecting and classifying breast lesions [10]. Visualization techniques such as Grad-CAM have also been employed to create visual explanations by highlighting the most significant regions an image to the model's decision [11]. Images may suffer from degradations such as resolution loss, blurring, and noise contamination, which can significantly alter the visual characteristics of breast tissue and may result in wrong diagnosis [12, 13]. Resolution is a fundamental characteristic of imaging systems determining the level of detail captured in the output image of the object under consideration. High-resolution images preserve fine structural details essential for detecting lesions, whereas low-resolution images may result in loss of critical information necessary for proper diagnosis. Similarly, image blurring caused by system optics, patient motion, or reconstruction processes reduces edge sharpness and contrast, thereby reducing important features. These artifacts in the images are commonly represented by Gaussian blur [14]. Another important factor affecting the image quality is the noise, which may arise from electronic components and acquisition conditions. Gaussian noise is widely used to simulate such type of degradations and has been shown to significantly impact feature extraction and classification performance [15, 16].

The development of deep learning has led to the advent of transformer-based CNNs models for efficiently capturing both local and global information required for accurate and reliable diagnosis. These models employ self-attention mechanism for estimating context dependent information [17]. Similarly, vision transformers, introduced by Alexey Dosovitskiy, have shown promising results in capturing long-range dependencies from the input images, particularly in medical diagnosis [18]. On the other hand, hybrid architectures use convolutional feature extraction with attention-based global reasoning for enhanced medical diagnosis [19]. The main discrepancies of such models are that they often require large datasets and high computational resources for the analysis. In real-world clinical environments, mammograms are acquired using different imaging systems with varying hardware configurations, detector technologies, and acquisition protocols resulting in distortions due to spatial resolution, contrast, noise levels, and sharpness. Hence, the usage of conventional machine learning systems in CAD results in the dependence of diagnostic reliability on the quality and consistency of the input images. Patch based learning mechanism using multi-scale strategies and hybrid architecture has been successfully applied and reported to enhance detection performance [20, 21]. Incorporation of patch based analysis in CAD systems may be expected to resolve some of the problems. Deep learning models are highly sensitive to parametric distribution shifts caused by such degradations and lead to significant performance drops when evaluated on images taken under non-ideal conditions [22, 23]. Although data augmentation technique such as noise injection, blur simulation, and resolution scaling may be employed to improve generalization, but do not provide a clear understanding of the dependence of the each degradation factor on model behaviour. Although, a controlled degradation framework has been investigated and reported in [24], but its application in mammogram analysis has not yet been explored particularly in patch based systems.

One of the most important features of the CAD systems is the interpretability for providing explanations of model decisions which may be achieved using attention mechanism by highlighting most important regions in the input images. Sophisticated attention modules like Grad-CAM, spatial, and channel-wise attention mechanisms, have been successfully employed to improve both performance and interpretability in medical imaging [25–27]. Despite significant progress, there are still several gaps to be explored. Most of the studies focus on improving classification accuracy under controlled imaging conditions ignoring robustness to real-world variability like resolution, blur, and noise. Mostly, these approaches operate at the full-image level, overlooking localized effects that are critical for detecting lesions. The correlation among different types of degradations and attention-based interpretability remains largely unexplored. Motivated by these challenges, the present research presents a comprehensive framework to systematically investigate the effect of degradations present in mammograms due to resolution variation, blurring, and additive Gaussian noise on attention guided patch-based mammogram cancer detection. The work is expected to reduce the gap between controlled research conditions and real-world clinical environments by providing a robust model under different degradation conditions. The outcomes of this research are expected to provide optimised image quality, particularly in rural and resource-limited clinical environment where there is limited access to advanced mammographic imaging systems.

2. MATERIAL AND METHOD

The literature survey showed that the performance of machine learning-based classification systems is significantly affected by the quality of the acquired images. In this research, three imaging degradations spatial resolution, Gaussian blur, and additive Gaussian noise are finalised to be investigated. For the investigations, the degradations are introduced in a systematic manner to imitate actual clinical acquisition conditions in mammography systems.

The overall methodology is shown in FIGURE 2. For investigating the sensitivity of the proposed model to specific imaging artefacts, each degradation factor is varied while keeping all other experimental conditions unchanged. The proposed system integrates five major stages: (i) dataset preparation and patch extraction, (ii) image pre-processing and degradation modelling, (iii) CNN-based feature extraction and classification using circular attention, (iv) controlled training and testing under varying imaging conditions, and (v) quantitative and qualitative performance evaluation. Informal experiments conducted in our preliminary investigations have shown that the performance ordering is circular attention > learned attention > no attention and hence, the same mechanism has been used in the present study. The process begins with mammogram acquisition and patch extraction, followed by preprocessing and simulation of degradations in the acquired images. The resultant breast image patches are subsequently analysed using the proposed attention-guided CNN. The model is trained using the labelled patches as cancerous and non-cancerous. The trained model is evaluated using standard performance metrics to identify the imaging degradations having the significant influence on the classification performance.

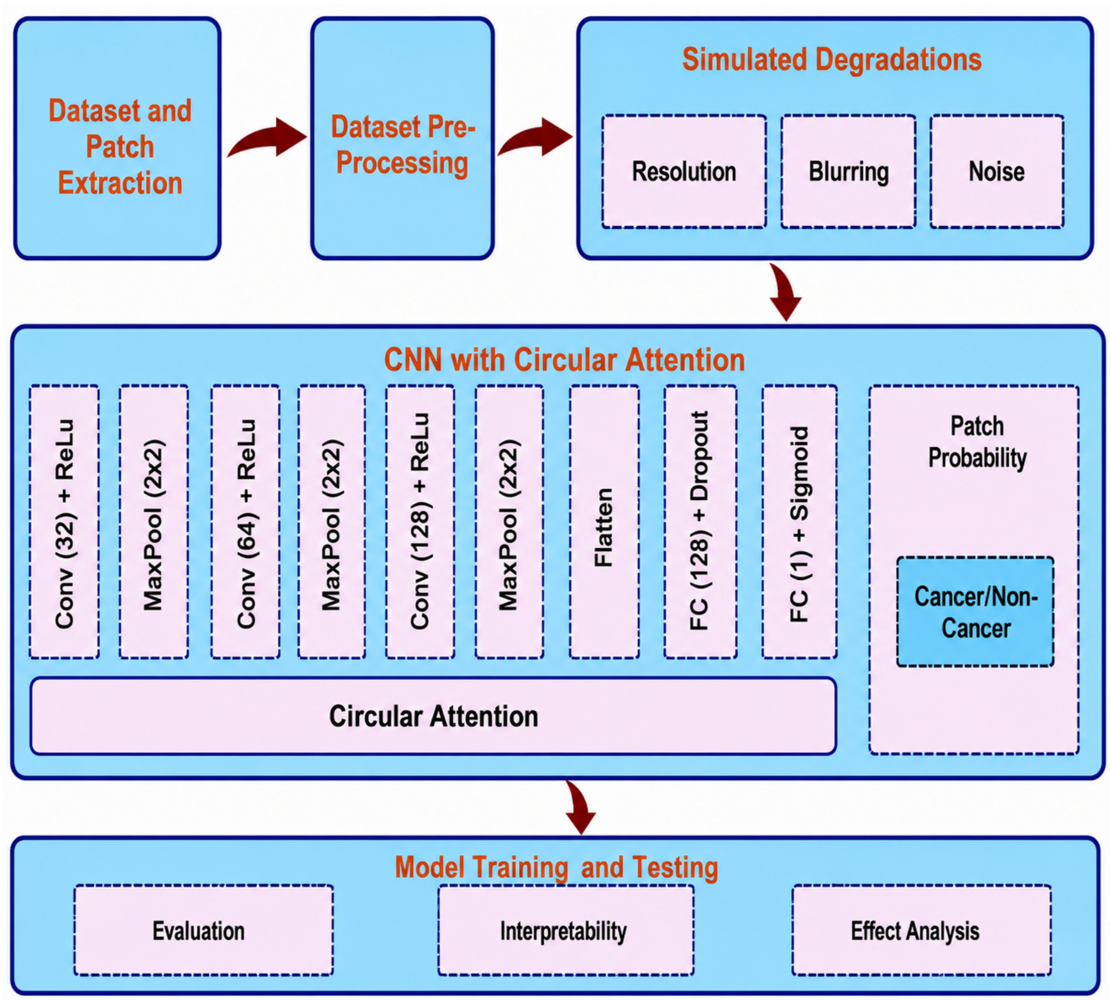

Figure 2: Proposed Robustness-Aware Framework for Investigating the Impact of Imaging System Characteristics on Patch-Based Mammogram Cancer Detection

The investigations were carried out using two publicly available breast images datasets: i) Curated Breast Imaging Subset of the Digital Database for Screening Mammography (CBIS-DDSM) dataset [28], ii) Invasive Ductal Carcinoma (IDC) dataset [29]. These datasets consists of annotated pathology-confirmed breast images categorized into cancerous and non-cancerous classes. The CBIS-DDSM dataset, a curated version of the Digital Database for Screening Mammography (DDSM), comprises high-resolution digitized mammograms with benign and malignant findings, along with associated metadata. On the other hand, the IDC dataset consists of 277,524 RGB image patches of size 50×50 pixels extracted from 162 hematoxylin and eosin (H&E)-stained breast histopathology specimens scanned at 40× magnification, each labelled as cancerous or non-cancerous.

Since breast abnormalities (masses, micro calcifications, and architectural distortions) are mostly locally confined, hence a patch-based strategy was implemented to facilitate localized feature extraction while maintaining computational efficiency. Initially, clinically relevant regions of interest (ROIs) of mammograms were selected from the annotated images and partitioned into fixed-size patches of 50×50 pixels, and every patch was assigned a binary label corresponding to cancerous or non-cancerous tissue based on pathological findings. This technique increases the effective number of training samples enabling the model to learn localized discriminative features with high accuracy and reduced computational complexity.

Pixel intensities of each patch were normalized to the range [-1,1] for stabilized training and convergence. A custom dataset class was used for image loading, transformation, and batch formation. Circular attention implemented by spatial weighting for prioritizing the most of the relevant parts of the patches has been used. Gaussian-like function is employed for estimating the attention mask. The function provides relatively more weights to central pixels and lower weights to peripheral region. The central region of the feature map determines the location of the abnormality.

Formally, a mammogram image $\mathbf{I}$ can be represented as: $\mathbf{I} = \{\mathbf{P}1, \mathbf{P}2, \mathbf{P}3, \ldots, \mathbf{P}?\}$ where $\mathbf{P}i$ denotes the ith image patch and n represents the total number of extracted patches. The dataset is divided into training, validation, and testing subsets as per the ratio 70:20:10. For testing of degradation robustness without any patch-level data leakage, the 10% samples from IDC dataset were converted to 50 × 50 sized patches and none of patch from this set was used during training or validation. Prior to training, all image patches are pre-processed using gray scale conversion, resizing (50×50), and intensity normalization using

$$\bar{\mathbf{P}}_i = (\mathbf{P}_i - I_{\min})/(I_{\max} - \mathbf{I}_{\min})$$

where Imin, and Imax represent the original minimum, and maximum intensity values, respectively. To simulate realistic imaging conditions, three major degradation factors are introduced: resolution, blur, and noise. Resolution degradation is simulated through a down sampling up sampling process:

$$\mathbf{P}'_i = U(D(\bar{\mathbf{P}}_i, s))$$

where $\bar{\mathbf{P}}_i$ is the original patch, $\mathbf{P}'_i$ is the degraded patch, and s represents the reduced spatial resolution. Patch resolution is varied from 50×50 pixels (original patch) down to 40×40 pixels, with detailed results reported for 45×45 and 40×40 pixels. Image blur is modelled using Gaussian convolution:

$\mathbf{P}'_i = \bar{\mathbf{P}}_i * G(\sigma, w)$ where $G(\sigma, w)$ denotes the Gaussian kernel of standard deviation $\sigma$and width. w. Lavel of blur is governed by the standard deviation (σ) rather than by the kernel width (for small σ the effective support of the Gaussian lies entirely within a 3×3 window); accordingly, the kernel size is fixed at 3×3 and experiments are reported for $\sigma = 0.3$ (slight blur) and $\sigma = 0.5$ (moderate blur). Noise degradation is introduced using additive Gaussian noise:

$$\mathbf{P}'_i = \bar{\mathbf{P}}_i + N(0, \sigma^2).$$

For investigating effect of additive Gaussian noise, SNR values of 30 dB, 20 dB, 10 dB, and 0 dB, representing low, moderate, high, and severe noise conditions, respectively have been used in the experiments. Following preprocessing and degradation simulation, image patches are analysed using a convolutional neural network integrated with a circular attention mechanism. The CNN architecture consists of three convolutional layers containing 32, 64, and 128 filters, respectively. Each convolutional layer is followed by ReLU activation and max-pooling operations. The extracted features are flattened and passed through fully connected layers with dropout regularization before binary classification is performed using a sigmoid activation function. To improve feature localization and interpretability, a circular attention mechanism is incorporated into the CNN architecture. The attention map is computed as

$$\mathbf{A} = \sigma(\mathbf{W}_2(\mathrm{ReLU}(\mathbf{W}_1(\mathbf{F}))))$$

where F represents the extracted feature map and W1 and W2 denote trainable parameters. The circular spatial weighting mask used for the investigations is defined as

$$M(x, y) = \exp(-((x - x_\mathrm{p})^2 + (y - y_\mathrm{p})^2)/(2r^2))$$

where (x_p, y_p) denotes the patch centre and r controls the spread of attention region. The final attention-weighted feature representation is obtained as

$$\mathbf{F}' = \mathbf{F} \odot (\mathbf{A}\mathring{u}\mathbf{M})$$

where $\odot$ denotes element-wise multiplication. The model is trained on original non-degraded mammogram patches to ensure that the learned feature representations correspond to ideal imaging conditions. Model parameters optimization is performed using the Binary Cross-Entropy (BCE) loss function. It quantifies the difference between the predicted class probabilities and the corresponding ground-truth labels as

$$L_{BCE} = -\frac{1}{N}\sum_{i=1}^{N}[y_i \log(p_i) + (1 - y_i)\log(1 - p_i)]$$

where L_{BCE} denotes the binary cross-entropy loss, N represents the total number of training samples, $y_i$is the ground-truth label of the i^{th}sample, and $p_i$is the probability predicted by the model. The ground-truth label is defined as

$$y_i = \begin{cases} 1, \text{ Cancerous} \\ 0, \text{ Non} - \text{cancerous} \end{cases}$$

The BCE loss assigns higher weightage to correct predictions while imposing larger penalties to incorrect predictions. The loss function is minimised through back propagation which progressively make the model to learn robust and discriminative features of cancerous and non-cancerous mammogram patches. The model parameters are optimized using the Adam optimizer with batch gradient descent, providing efficient convergence and stable optimization. During each training epoch, batches of mammogram patches are sent through the model to generate prediction probabilities and there after the BCE loss are estimated. The resulting gradients are propagated backward allowing continuous adjustment of the model weights. The model is trained for 101 epochs using a batch size of 64 for high computational efficiency, convergence stability, and generalization performance. After training, the learned model is evaluated under multiple degradation conditions to investigate its performance against variations in image quality.

Performance evaluation of the proposed system is carried out at both the patch level and the image level using accuracy, precision, recall, F1 score, specificity, and the area under the receiver operating characteristic curve (ROC-AUC). Furthermore, confusion matrix analysis is analysed to quantify True Positives (TP), True Negatives (TN), False Positives (FP), and False Negatives (FN), thereby providing detailed insight into the classification behaviour and error characteristics of the proposed model. Image-level analysis is carried out by aggregating the predictions from all constituent patches, thereby resulting in a diagnosis for the input mammogram or the given tissue. To gain insight of the attention mechanism, attention maps generated by the circular attention module are superimposed over the corresponding mammogram patches. These visual details help in identifying the significant regions of the mammogram patches for efficient decision-making. Finally, a comprehensive degradation-specific analysis is carried out by comparing the classification performance of the trained model across different levels of resolution, blur, and additive Gaussian noise for identifying different factors that strongly influence breast cancer classification performance.

3. RESULTS AND DISCUSSION

The section presents a comprehensive evaluation of the proposed circular attention guided CNN for patch-based mammogram for cancer detection under different types of degradations introduced by the imaging system and the environmental conditions. As explained in the Material and Method section, effect of three major image degradations, namely resolution, Gaussian blur, and additive Gaussian noise, on the classification accuracy, robustness, and generalization capability of the proposed model has been investigated. The model is trained on high-quality, non-degraded mammogram patches, while during testing patches with different degradations have been used. To investigate the effectiveness of the optimization strategy and the convergence behaviour during training, variation of BCE loss, accuracy, precision, and recall over successive epochs (FIGURE 3) have been analysed.

The training and validation loss curves (FIGURE 3a) show exponential reduction throughout the training, confirming that the model continuously minimizes the BCE loss by learning discriminative features. Higher loss values during the initial training phase are because of the random initialization of model parameters. As training progresses, the loss decreases and gradually approaches a stable minimum, indicating effective convergence of the network optimization. The close correspondence between the training and validation loss curves shows that the proposed model learns generalized features without over fitting or unstable optimization behaviour. Similarly, the classification accuracy (FIGURE 3b) is relatively low at the beginning of training, as the model has limited knowledge of the discriminative features for deciding whether the input patch is cancerous or non-cancerous. Successive parameters update results in effective patch classification as both accuracy curves increase steadily and eventually stabilize. The proposed model maintains a good balance between learning of new features and generalizing to previously unseen data, thereby confirming its robustness and reliability. The classification behaviour of the proposed model is also investigated through precision and recall curves (FIGURE 3c). It may be observed that the precision shows a gradual increase during training, indicating progressive reduction of false-positive predictions, improving the reliability of cancerous patch identification. Similarly, gradually increasing recall demonstrates enhanced capability to correctly detect cancerous mammogram patches while minimizing false-negative detection rate. The closeness of precision and recall curves indicates the effectiveness of the circular attention mechanism for achieving a balanced classification performance. The simultaneous convergence of the loss, accuracy, precision, and recall curves indicates the effectiveness of the proposed model. Smooth convergence, closeness between training and validation metrics, and stable performance of curves at the final training epochs collectively indicate efficient optimization, strong generalization capability, and reliable feature learning as shown in TABLE 1. ROC analysis

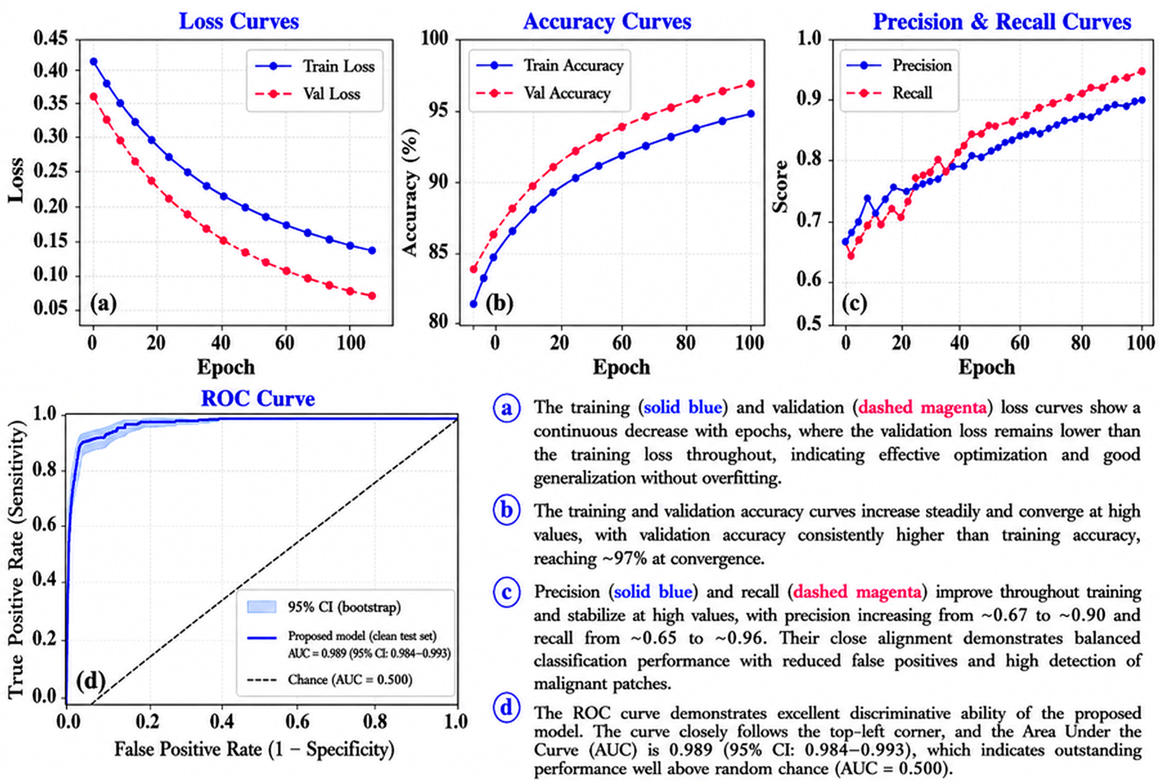

Figure 3: Performance analysis using training loss, accuracy, and, precision, recall, and ROC-AUC curves.

Table 1: Performance metrics of the proposed model

Metric	**Value (%)**	**Description**
Accuracy	97.0	Overall classification accuracy
Precision	92.0	Correct positive predictions
Recall	96.0	Cancer detection rate
F1-Score	94.8	Precision–recall balance
Specificity	97.0	Correct negative predictions
ROC-AUC	98.9	Area under ROC curve (95% CI: 98.4–99.3)

of the trained model shows an area under the curve as 0.989 (95% CI: 0.984–0.993, bootstrap with 1,000 resamples), confirming near-ceiling threshold-independent discrimination between cancerous and non-cancerous patches under ideal imaging conditions (FIGURE 3(d)).

Following the training, the model was systematically evaluated under varying imaging condition by independently varying resolution, Gaussian blur, and additive Gaussian noise while maintaining all remaining imaging parameters unchanged. For each degradation type, the results are compared with the corresponding baseline performance achieved using non-degraded mammogram patches for detailed evaluation of the robustness, sensitivity, and generalization capability of the proposed model under realistic imaging conditions. The effect of the degradations on the model performance is presented in the following sub sections. Because of the limited space in the paper, results are shown for four representative samples, sample no 8863 (979 patches; 207 cancerous) for the resolution study, sample no 8867 (1,642 patches; 162 cancerous) for the blur study, and sample no 8913 (955 patches; 82 cancerous) for the noise study. Sample no 8914 (1,098 patches; 120 cancerous) has been used for cross-image verification.

3.1 Resolution Effect

Resolution directly determines the fine anatomical and pathological structures, including lesion boundaries; micro calcifications, speculations, and subtle texture variations, hence may be expected to have maximum effect on the classification of cancerous and non-cancerous patches. To quantify the effect of resolution, the proposed circular attention-based CNN model was evaluated using both the original image resolution (50 × 50 pixels) and a simulated lower-resolution (45 × 45 pixels). FIGURE 4 presents a comparison of the model performance under two resolution conditions using spatial prediction maps, confusion matrices, representative attention maps, and quantitative attention-weights analysis, while TABLE 2 summarizes the resultant attention weights response of the attention mechanism. The analysis of the results provides both quantitative and qualitative evidence of degradation effects on classification performance.

The spatial prediction maps shown in FIGURE 4(a) and FIGURE 4(b) provide insight into the distribution of correctly and incorrectly classified patches across the whole mammogram tissue. At the original resolution (50 × 50 pixels), the cancerous region is characterized by a dense cluster of correctly classified cancerous patches with a few isolated false-negative predictions. The spatial continuity of correctly predicted patches shows that neighbouring cancerous patches preserve similar discriminative features and are correctly identified by the model. The spatial continuity of correct predictions indicates that neighbouring cancerous patches share similar discriminative features under ideal imaging conditions. The effect of resolution reduction on classification performance is shown by the confusion matrices (FIGURE 4(c) and FIGURE 4(d)). For (50 × 50 pixels) resolution, model correctly identifies 205 cancerous patches while producing only 2 false-negative predictions, demonstrating satisfactory sensitivity and reliable discrimination between cancerous and non- cancerous patches. The large number of correctly classified cancer patches indicates that the model has extracted sufficient spatial information required for accurate classification. Also, the relatively small number of false classifications shows that the classification pipeline operates reliably when high-resolution information is preserved in the patches. Slightly different behaviour is observed when the resolution is reduced to 45 × 45 pixels. The number of correctly detected cancer patches decreases from 205 to only 19, whereas the number of false-negative predictions increases from 2 to 188. Reducing the resolution to 40 × 40 pixels gives only 9 correctly detected cancerous patches and 198 false negatives. Importantly, the ROC-AUC collapses from 0.990 (95% CI: 0.985–0.993) at the original resolution to 0.823 (0.788–0.857) at 45 × 45 resolution (TABLE 3). At 40 × 40, the ROC-AUC comes as 0.753 (0.713–0.794, demonstrating that resolution degradation hampers the discriminative ability of the model. The decline in sensitivity indicates failure of model to recognize a large proportion of cancerous patches in low resolution images. As the number of correctly classified non-cancerous patches remains comparatively high, increase in missed cancer detection indicates more sensitive to spatial resolution of the cancerous patches. The attention maps also show effect of low resolution on weights as illustrated in FIGURE 4(e) and FIGURE 4(f). For the original 50 × 50 patches, the attention

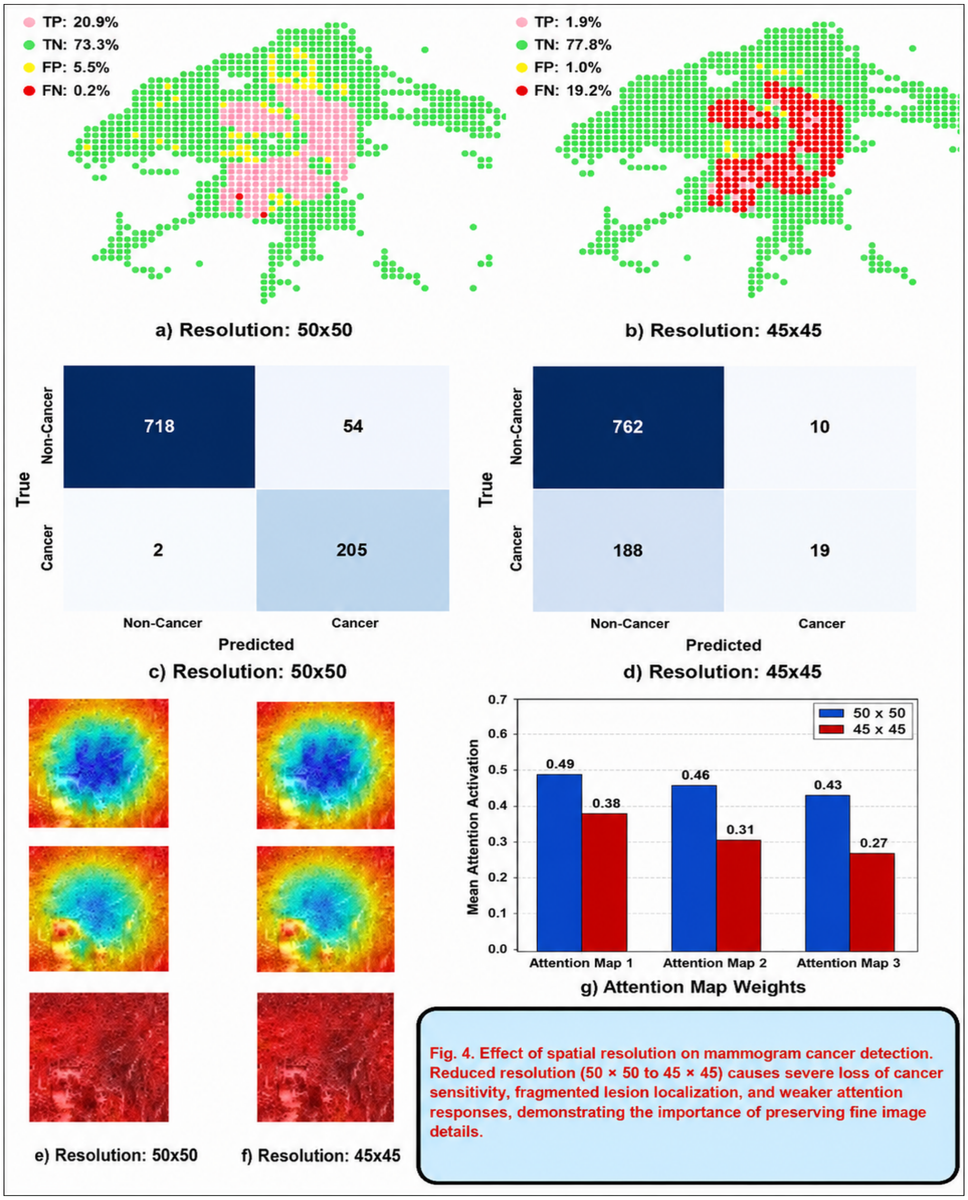

Figure 4: Effect of spatial resolution on mammogram cancer detection. Reduced resolution (50 × 50 to 45 × 45) causes severe loss of cancer sensitivity, fragmented lesion localization, and weaker attention responses, demonstrating the importance of preserving fine image details.

Table 2: Effect of resolution on resultant attention weights response of the attention mechanism

Resolution	Attention Map 1	Attention Map 2	Attention Map 3	Overall Attention Strength	Observation
50 × 50	0.49	0.46	0.43	0.46	Strong and localized attention responses with high confidence
45 × 45	0.38	0.31	0.27	0.32	Significant reduction in activation intensity and diffuse attention patterns

Table 3: Effect of resolution degradation on classification performance (using patch no 8863; 979 patches, 207 cancerous).

Condition	TP	FN	FP	TN	Accuracy	Precision	Recall	Specificity	F1	ROC-AUC (95% CI)
50×50 (original)	205	2	54	718	0.943	0.792	0.990	0.930	0.880	0.990 (0.985–0.993)
45×45	19	188	10	762	0.798	0.655	0.092	0.987	0.161	0.823 (0.788–0.857)
40×40	9	198	6	766	0.792	0.600	0.043	0.992	0.081	0.753 (0.713–0.794)

maps display a strong, compact, and highly concentrated central region indicating successful identification of important tissue structures resulting in higher attention weights. The attention maps for low resolution (45 × 45) result in weaker and more diffuse weights, thereby, unable to identify reliable discriminative cues.

3.2 BLURRING EFFECT

The presence of blurring generally simulated as Gaussian functions in mammographic images may be attributed detector limitations, patient motion during image acquisition, reconstruction algorithms, or post-processing operations. Although spatial resolution permanently removes image information through down sampling, Gaussian blurring mostly suppresses high-frequency components from the images reducing the edge sharpness, lesion boundaries, and fine texture patterns. Blurring modifies the fine structures of the image and thereby, reduces the discriminative information available for deep feature extraction. The proposed model was evaluated under different amounts of Gaussian blur by varying the standard deviation σ with the kernel size fixed at 3×3, since blur severity is governed by σ rather than by the kernel width (kernel sizes 3 and 9 at equal

σ were verified to produce statistically indistinguishable results). FIGURE 5 presents the results obtained

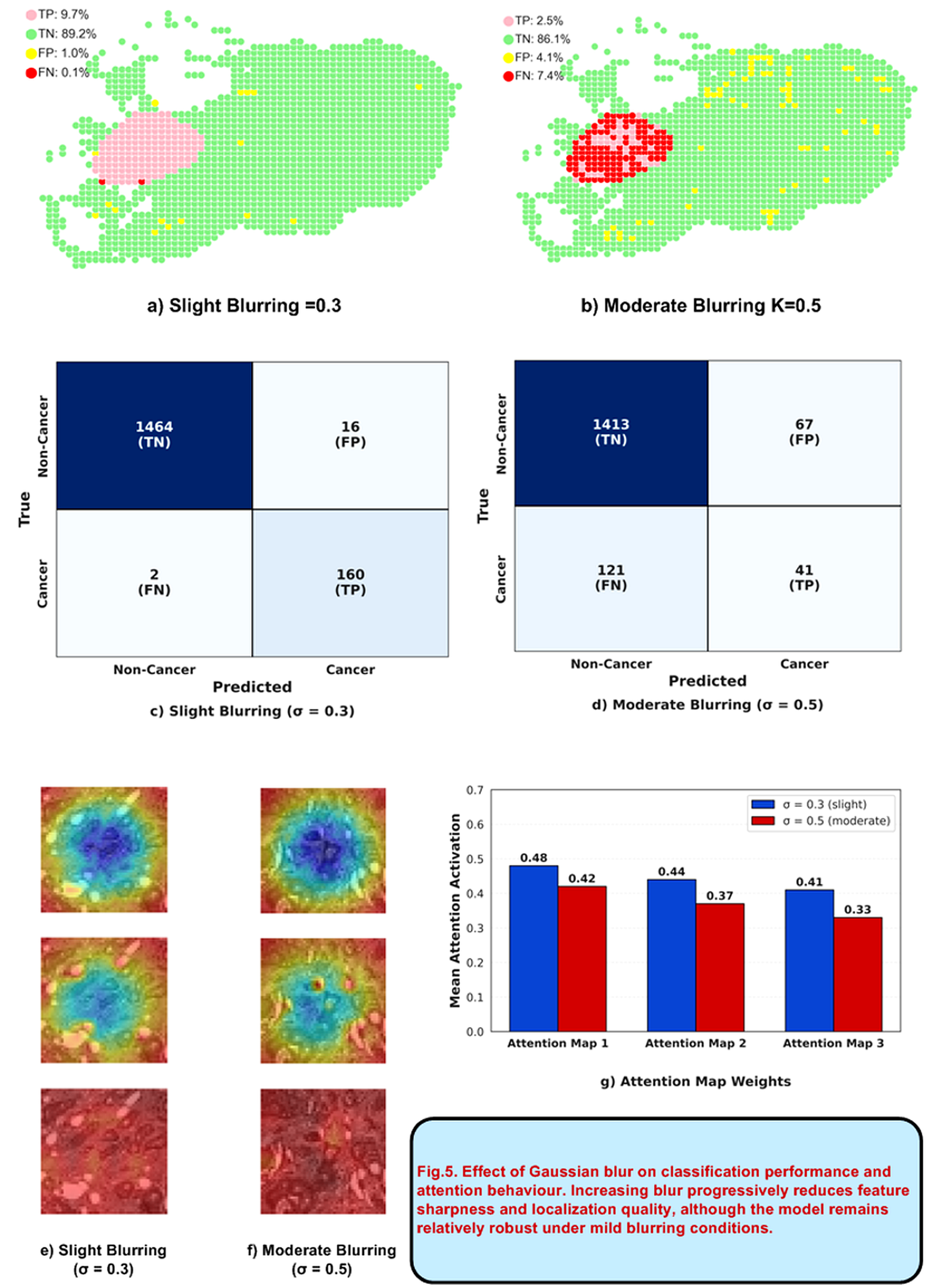

Figure 5: Effect of Gaussian blur on classification performance and attention behaviour. Increasing blur progressively reduces feature sharpness and localization quality, although the model remains relatively robust under mild blurring conditions.

for σ = 0.3 (slight blur) and σ = 0.5 (moderate blur). The results show the corresponding spatial prediction maps, confusion matrices, attention maps, and histograms based analysis of attention-weights. The quantitative analysis of attention weights is summarized in TABLE 4.

Table 4: Effect of blurring on classification performance

Blur Level	Attention Map 1	Attention Map 2	Attention Map 3	Overall Attention Strength	Observation
σ = 0.3 (slight)	0.48	0.44	0.41	0.44	Attention remains highly focused with minimal degradation
σ = 0.5 (moderate)	0.42	0.37	0.33	0.37	Reduced activation strength and less precise feature localization

The spatial prediction maps (FIGURE 5(a) and FIGURE 5(b)) show that under slight blur the model confines correctly classified patches within the lesion boundaries, with sparse false predictions near the lesion margins, whereas under moderate blur the correctly detected cancerous patches become sparse and a large fraction of the lesion is missed. Increasing σ beyond 0.5 showed unsatisfactory results. The analysis of the confusion matrices (FIGURE 5(c) and FIGURE 5(d)) shows that under slight blur (σ = 0.3), out of 1,480 non-cancerous patches and 162 cancerous patches, the model correctly classifies 1,464 non-cancer patches and 160 cancer patches, producing only 16 false-positive and 2 false-negative predictions, almost identical to the non-degraded baseline, with ROC-AUC = 0.998 (95% CI: 0.996–0.999). Under moderate blur (σ = 0.5), the re-verified results (TABLE 5) show a substantial degradation: correctly detected cancerous patches fall to 41 while false negatives rise to 121 (recall 0.25) and false positives increase to 67, with ROC-AUC reduced to 0.797 (0.762–0.832). With resolution reduction, the errors are dominated by missed cancerous patches, consistent with the suppression of the fine, high-frequency texture on which the model relies. In parallel, the attention maps shown in FIGURE 5(e) and FIGURE 5(f) reveal significant changes in the internal feature-learning process. For K = 3, the attention mechanism generates compact and well-localized activation patterns concentrated around diagnostically relevant tissue structures. As σ approaches 0.5, the lesion regions become less concentrated and more diffused, indicating reduced confidence in localizing discriminative lesion features. The smoothing of lesion boundaries weakens the high-frequency image components available for accurate feature extraction, and results in broader attention responses. The histogram based analysis of attention-weights (FIGURE 5(g)) and summarized in TABLE 4. For slight blur (σ = 0.3), the mean activation values for attention maps 1, 2, and 3 are 0.48, 0.44, and 0.41, respectively, resulting in an overall attention strength of 0.44, whereas moderate blur (σ = 0.5) reduces the corresponding activation values to 0.42, 0.37, and 0.33, yielding an overall attention strength of 0.37. The reduction of activation values indicates that Gaussian blurring weakens the confidence of the circular attention module in identifying diagnostically relevant regions, even though the final classification performance remains almost unaffected.

The analysis shows that the model is robust to slight Gaussian blurring ($\sigma = 0.3$), preserving sensitivity and specificity, whereas moderate blur ($\sigma = 0.5$) produces a resolution-like collapse of sensitivity and of the discriminative ability of the model. This robustness is particularly important for practical

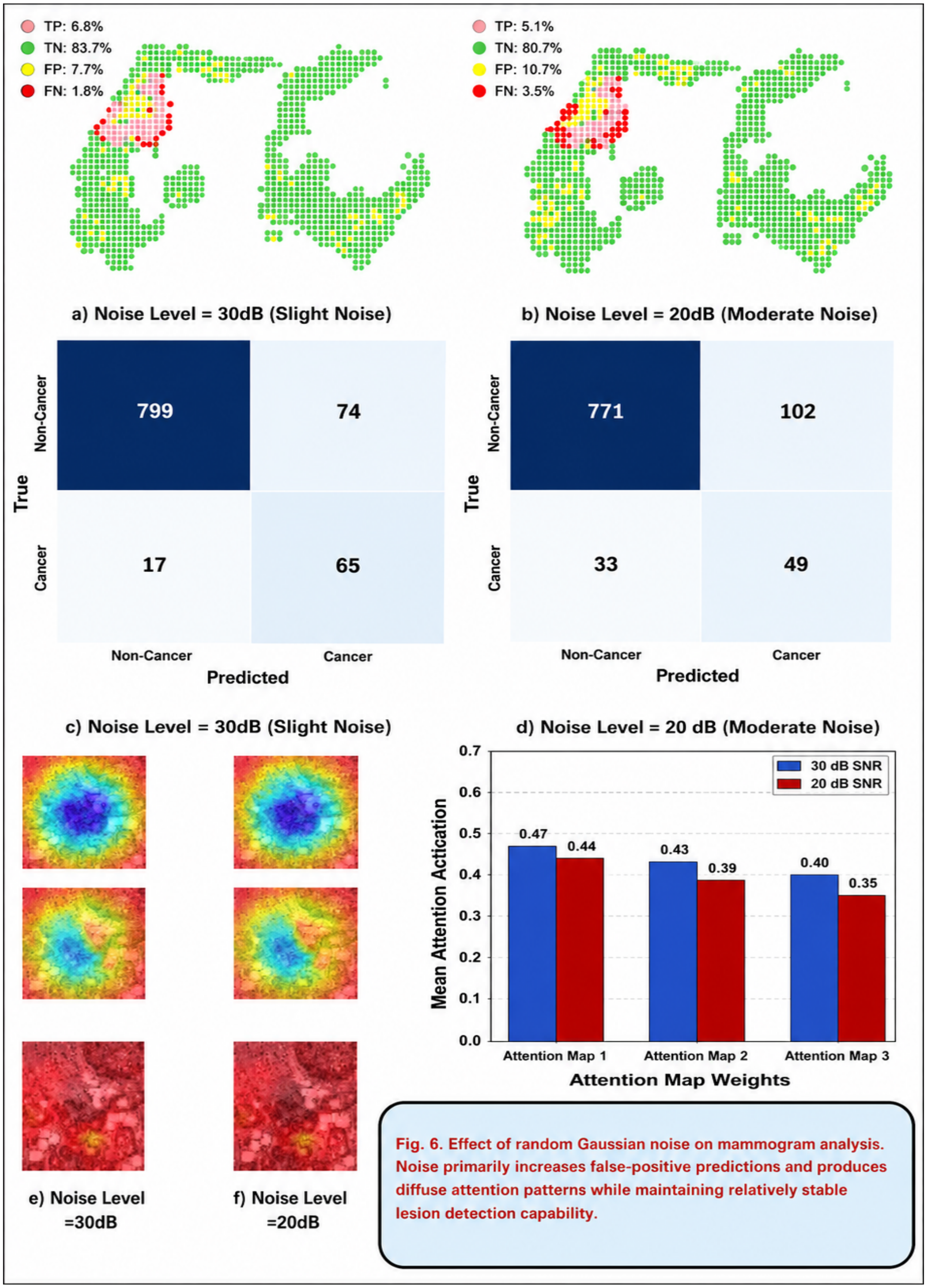

Figure 6: Effect of random Gaussian noise on mammogram analysis. Noise primarily increases false-positive predictions and produces diffuse attention patterns while maintaining relatively stable lesion detection capability.

Table 5: Effect of Gaussian blur on classification performance (held-out source image 8867; 1,642 patches, 162 cancerous). Kernel fixed at 3×3.

Condition	**TP**	**FN**	**FP**	**TN**	**Accuracy**	**Precision**	**Recall**	**Specificity**	**F1**	**ROC-AUC (95% CI)**
No blur	160	2	16	1464	0.989	0.909	0.988	0.989	0.947	0.999 (0.997–0.999)
σ = 0.3 (slight)	160	2	16	1464	0.989	0.909	0.988	0.989	0.947	0.998 (0.996–0.999)
σ = 0.5 (moderate)	41	121	67	1413	0.886	0.380	0.253	0.955	0.304	0.797 (0.762–0.832)

clinical imaging systems, where mild blur caused by acquisition or reconstruction processes is often unavoidable.

3.3 EFFECT OF GUASSIAN RANDOM NOISE

The noise introduced by sensors, signal acquisition, analog-to-digital conversion, and low-dose imaging protocols is generally unavoidable in mammographic imaging systems and results in stochastic intensity fluctuations throughout the image. The fluctuations modify local contrast, lesion structure, and texture patterns that may interfere in feature extraction process. Experiments were conducted by varying the additive Gaussian noise over SNR levels of 30, 20, 10, and 0 dB with a fixed random seed (42). FIGURE 6 presents the results for two representative noise levels, i.e. 30 dB (slight noise) and 20 dB (moderate noise). Corresponding spatial prediction maps, confusion

Table 6: Effect of noise on classification performance.

Noise Level	**Attention Map 1**	**Attention Map 2**	**Attention Map 3**	**Overall Attention Strength**	**Observation**
30 dB SNR	0.47	0.43	0.40	0.43	Stable attention with strong lesion-focused activations
20 dB SNR	0.44	0.39	0.35	0.39	More diffuse attention and increased uncertainty due to noise artifacts

Table 7: Effect of additive Gaussian noise on classification performance (using sample no 8913; 955 patches, 82 cancerous).

Condition	TP	FN	FP	TN	Accuracy	Precision	Recall	Specificity	F1	ROC-AUC (95% CI)
No noise	81	1	42	831	0.955	0.659	0.988	0.952	0.790	0.995 (0.991–0.997)
30 dB	65	17	74	799	0.905	0.468	0.793	0.915	0.588	0.945 (0.920–0.967)
20 dB	49	33	102	771	0.859	0.325	0.598	0.883	0.421	0.848 (0.800–0.888)
10 dB	60	22	238	635	0.728	0.201	0.732	0.727	0.316	0.775 (0.716–0.825)
0 dB	0	82	0	873	0.914	0.000	0.000	1.000	0.000	0.500 (0.500–0.500)

matrices, attention maps, and histogram based attention-weight analysis are also shown in the figure. TABLE 6 summarizes the quantitative attention responses under both noise levels.

The spatial prediction maps (FIGURE 6(a) and FIGURE 6(b)) show that at 30 dB noise, the model correctly detects cancerous patches and the detected patches remain concentrated within the lesion region, forming a compact well defined coherent cluster. A few false-positive predictions are distributed in the periphery of the lesion showing spatial continuity of the lesion in the presence of slight noise. At 20 dB, the overall lesion remains broadly identified; however, the number of false-positive patches outside the lesion increases sharply. Sparsely distributed false-positive responses suggest that the noise introduces random intensity variations that partially resemble lesion texture which reduces the discrimination between cancerous and non-cancerous regions. The confusion matrices shown in FIGURE 6(c) and FIGURE 6(d) demonstrate the graded effect of noise (TABLE 7). Out of a total of 873 non-cancerous and 82 cancerous patches, the model correctly classifies 799 non-cancer and 65 cancer patches at 30 dB SNR, producing 74 false-positive and 17 false-negative predictions (ROC-AUC = 0.945, 95% CI: 0.920–0.967). At 20 dB, true positives decrease to 49 while false positives increase to 102 (ROC-AUC = 0.848, 0.800–0.888); at 10 dB, false positives grow further to 238 although 60 cancerous patches are still detected (ROC-AUC = 0.775). In contrast to resolution and blur, whose errors are dominated by missed cancers, the noise-induced errors are dominated by false positives: random intensity fluctuations in healthy tissue increasingly mimic suspicious texture, so noise primarily erodes specificity while sensitivity degrades more gradually. At 0 dB the model predicts every patch as non-cancerous; accuracy nevertheless reads 91.4% owing to class imbalance, while ROC-AUC = 0.500 correctly reveals the complete loss of discrimination — illustrating why threshold-independent metrics are indispensable in this analysis. The attention maps (FIGURE 6e and FIGURE 6f) show that for 30 dB, the model generates strong and well-localized patterns around the lesion. At 20 dB, the maps become more diffused and less localized, although the lesion region continues to receive the strongest activation. Attention responses appearing in normal tissue indicates that noise-induced fluctuations results in uncertainty in reliable feature extraction. The histogram based attention-weight analysis is shown in FIGURE 6(g) and summarized in TABLE 6. It is clear from the table that at 30 dB noise, the mean activation values for attention maps 1, 2, and 3 are 0.47, 0.43, and 0.40, respectively, producing overall attention strength of 0.43. The noise level of 20 dB results in decreased activation values of 0.44, 0.39, and 0.35. For these attention weights, the overall attention strength is relatively modest (0.39). The observations show a gradual reduction in attention selectivity with increasing noise intensity. The analysis of the proposed model under different noise levels highlights the effectiveness of the attention mechanism in preserving discriminative features. The lesion morphology remains largely preserved, allowing the model to maintain high cancer detection sensitivity. Below 20 dB, the noise introduces random texture patterns resulting in reduced contrast between non-cancerous and cancerous regions, culminating in the complete loss of discrimination at 0 dB.

4. CONCLUSIONS AND FUTURE SCOPE

This study presented the results of the experiments conducted for investigating the effect of degradations on attention-guided patch-based machine learning mammographic systems. The experiments carried out for investigating the effect of 3 degradations, resolution, blurring, and Gaussian noise introduced by the mammographic imaging systems in patch-based machine learning demonstrate that imaging system parameters have a noticeable effect on its performance. Resolution had the most severe effect on the classification performance. Reducing patch resolution from 50×50 to 45×45 pixels resulted in a sharp decrease in sensitivity, with correctly detected cancerous patches falling from 205 to 19, false negative detections rising from 2 to 188, ROC-AUC collapsing from 0.990 to 0.823 (and further to 0.753 at 40×40), attention strength decreasing from 0.46 to 0.32, and the attention maps shifting from compact and localized to weak and diffuse patterns. Fine-grained structures like micro calcifications and speculated margins, which are essential for accurate classification, are lost at the reduced resolution. Blurring exhibited a graded effect on classification performance. Under slight Gaussian blur ($\sigma = 0.3$), sensitivity, specificity, and ROC-AUC remained essentially unchanged, whereas moderate blur ($\sigma = 0.5$) produced a resolution-like collapse of sensitivity (recall $0.99 \rightarrow 0.25$; ROC-AUC $0.999 \rightarrow 0.797$). With increasing blur, the attention strength decreased from 0.44 to 0.37 and the activation maps became visibly less concentrated around the central portion of the lesions. Although the classification accuracy is not considerably affected, the blurring affects the model's internal weights and thereby affecting the interpretability of its decisions. On the other hand, Gaussian noise mainly affected specificity rather than sensitivity as the SNR decreased from 30 dB to 10 dB (ROC-AUC $0.945 \rightarrow 0.775$ on image 8913): false-positive predictions grew progressively while cancer sensitivity degraded more gradually, and the attention strength decreased from 0.43 to 0.39, making activation patterns diffuse and noisy. At 0 dB, discrimination was lost entirely (ROC-AUC = 0.500) although accuracy remained above 87% due to class imbalance, underscoring the importance of threshold-independent evaluation.

The investigations showed that resolution reduction is the most damaging, moderate blurring is intermediate, slight blurring is harmless, and additive noise degrades performance gradually with decreasing SNR. The study contributes towards the development of more robust and interpretable computer-aided breast cancer analysis systems; subject to the limitations discussed above and to future clinical validation, such robustness characterization may ultimately support deployment in rural and resource-constrained healthcare settings, where access to high-end imaging infrastructure is often limited. The framework can be extended to hybrid CNN transformer architectures, full-field digital mammograms, Digital Breast Tomosynthesis (DBT), and multimodal breast imaging datasets, incorporating uncertainty-aware and explainable machine learning techniques to strengthen the clinical reliability of automated breast cancer diagnosis systems.

References

[1] Hinton G, Deng L, Yu D, Dahl GE, Mohamed A, et al. Deep Neural Networks for Acoustic Modeling in Speech Recognition: The Shared Views of Four Research Groups. IEEE Signal Process Mag. 2012;29:82-97.

[2] LeCun Y, Bottou L, Bengio Y, Haffner P. Gradient-Based Learning Applied to Document Recognition. Proc IEEE. Nov. 1998;86:2278-2324.

[3] He K, Zhang X, Ren S, Sun J. Deep Residual Learning for Image Recognition. Proceedings of the IEEE conference on computer vision and pattern recognition. 2016:770-778.

[4] He K, Zhang X, Ren S, Sun J. Identity Mappings in Deep Residual Networks. In European conference on computer vision. Cham: Springer International Publishing. 2016:630-645.

[5] Huang G, Liu Z, van der Maaten L, Weinberger KQ. Densely Connected Convolutional Networks. In 2017 IEEE conference on computer vision and pattern recognition (CVPR). IEEE. 2017:2261-2269.

[6] Ehteshami Bejnordi B, Veta M, Johannes van Diest P, van Ginneken B, Karssemeijer N, et al. Diagnostic Assessment of Deep Learning Algorithms for Detection of Lymph Node Metastases in Women With Breast Cancer. JAMA. 2017;318:2199-2210.

[7] Nasser M, Yusof UK. Deep Learning Based Methods for Breast Cancer Diagnosis: A Systematic Review and Future Direction. Diagnostics. 2023;13:161.

[8] Srinidhi CL, Ciga O, Martel AL. Deep Neural Network Models for Computational Histopathology: A Survey. Med Image Anal. 2021;67:101813.

[9] Yan R, Ren F, Wang Z, Wang L, Zhang T, et al. Breast Cancer Histopathological Image Classification Using a Hybrid Deep Neural Network. Methods. 2020;173:52-60.

[10] Ribli D, Horváth A, Unger Z, Pollner P, Csabai I. Detecting and Classifying Lesions in Mammograms With Deep Learning. Sci Rep. 2018;8:4165.

[11] Selvaraju RR, Cogswell M, Das A, Vedantam R, Parikh D, et al. Grad-CAM: Visual Explanations From Deep Networks. Proceedings of the IEEE international conference on computer vision. 2017:618-626.

[12] Armato SG III, McLennan G, Bidaut L, McNitt-Gray MF, Meyer CR, et al. The Lung Image Database Consortium (Lidc) and Image Database Resource Initiative (Idri): A Completed Reference Database of Lung Nodules on CT Scans. Med Phys. 2011;38:915-931.

[13] Hendrycks D, Dietterich T. Benchmarking Neural Network Robustness to Common Corruptions and Perturbations. 2019. ArXiv preprint: https://arxiv.org/pdf/1903.12261

[14] Gonzalez RC, Woods RE. Digital Image Processing, 4th ed. Upper Saddle River, NJ, USA: Pearson. 2018.

[15] Jain AK. Fundamentals of Digital Image Processing. Englewood Cliffs. Prentice-Hall, Inc. 1989.

[16] Hendrycks D, Mazeika M, Wilson D, Gimpel K. Using Trusted Data to Train Deep Networks on Labels Corrupted by Severe Noise. Adv Neural Inf Process Syst. 2018;31.

[17] Vaswani A, Shazeer N, Parmar N et al. Attention Is All You Need. In: Proceedings of the NeurIPS. 2017.

[18] Dosovitskiy A, Beyer L, Kolesnikov A, Weissenborn D, Zhai X, et al. An Image Is Worth 16×16 Words: Transformers for Image Recognition at Scale. International Conference on Learning Representations. 2021.

[19] Chen J, Lu Y, Yu Q, Luo X, Adeli E, Wang Y, Lu L, Yuille AL, Zhou Y. TransUNet: Transformers Make Strong Encoders for Medical Image Segmentation. 2021. ArXiv preprint: https://arxiv.org/pdf/2102.04306

[20] Roy K, Banik D, Bhattacharjee D, Nasipuri M. Patch-Based System for Classification of Breast Histology Images Using Deep Learning. Comput. Med. Imaging Graph. 2019;71:90-103.

[21] Lotter W, Sorensen G, Cox D. A Multi-Scale CNN and Curriculum Learning Strategy for Mammogram Classification. In International Workshop on Deep Learning in Medical Image Analysis. Cham: Springer International Publishing. 2017:169-77.

[22] Dodge S, Karam L. Understanding How Image Quality Affects Deep Neural Networks. In2016 eighth international conference on quality of multimedia experience (QoMEX). IEEE. 2016:1-6.

[23] H. Guan and M. Liu. Domain Adaptation for Medical Image Analysis: A Survey. IEEE Trans. Biomed. Eng. vol. 2022; 69:1173–1185.

[24] Jaspers TJ, Boers TG, Kusters CH, Jong MR, Jukema JB, De Groof AJ, Bergman JJ, de With PH, van der Sommen F. Robustness Evaluation of Deep Neural Networks for Endoscopic Image Analysis: Insights and Strategies. Med. Image Anal. 2024;94:103157.

[25] Schlemper J, Oktay O, Schaap M, Heinrich MP, Kainz B, et al. Attention Gated Networks: Learning to Leverage Salient Regions in Medical Images. Med Image Anal. 2019;53:197-207.

[26] Xie Y, Yang B, Guan Q, Zhang J, Wu Q, Xia Y. Attention Mechanisms in Medical Image Segmentation: A Survey. 2023. ArXiv preprint: https://arxiv.org/pdf/2305.17937

[27] kaba Gurmessa D, Jimma W. Jimma. Explainable Machine Learning for Breast Cancer Diagnosis From Mammography and Ultrasound Images: A Systematic Review. BMJ Health & Care Informatics. 2024;31:e100954.

[28] https://www.kaggle.com/datasets/awsaf49/cbis-ddsm-breast-cancer-image-dataset.

[29] https://www.ncbi.nlm.nih.gov/